Cell Reports

Article

Lon degrades stable substrates slowly but with enhanced processivity, redefining the attributes of a successful AAA+ protease

Graphical abstract

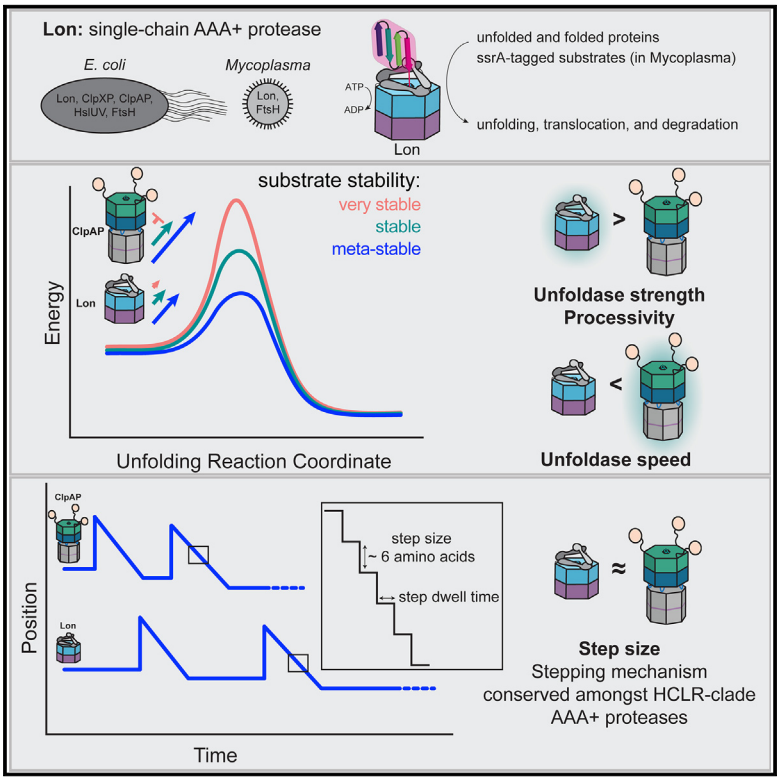

Highlights

- Single-molecule studies of *M. florum* Lon reveal it is slower than other proteases
- *Mf*Lon translocates substrates with a step size of ~6 residues per ATP hydrolyzed
- HCLR-clade AAA+ proteases share a conserved ATP-driven translocation mechanism
- *Mf*Lon is highly processive while degrading even stable multi-domain substrates

Authors

Meghann R. Kasal, Hema Chandra Kotamarthi, Madeline M. Johnson, Hannah M. Stephens, Matthew J. Lang, Robert T. Sauer, Tania A. Baker

Correspondence

tabaker@mit.edu

In brief

Kasal et al. perform single-molecule characterizations of Lon protease using the bacterial enzyme from *Mesoplasma florum* and discover that distinct subfamilies of the HCLR-clade AAA+ unfoldases use a conserved ATP-driven translocation mechanism. Furthermore, Lon is highly processive and a powerful unfoldase that appears tuned to degrade substrates to completion.

Kasal et al., 2023, Cell Reports *42*, 113061
September 26, 2023
https://doi.org/10.1016/j.celrep.2023.113061

CellPress

Cell Reports

CellPress
OPEN ACCESS

Article

Lon degrades stable substrates slowly but with enhanced processivity, redefining the attributes of a successful AAA+ protease

Meghann R. Kasal,[1] Hema Chandra Kotamarthi,[1] Madeline M. Johnson,[2] Hannah M. Stephens,[2] Matthew J. Lang,[2] Robert T. Sauer,[1] and Tania A. Baker[1,3,*]

[1]Department of Biology, Massachusetts Institute of Technology, Cambridge, MA 02139, USA
[2]Department of Chemical and Biomolecular Engineering, Vanderbilt University, Nashville, TN 37235, USA
[3]Lead contact
*Correspondence: tabaker@mit.edu
https://doi.org/10.1016/j.celrep.2023.113061

SUMMARY

Lon is a widely distributed AAA+ (ATPases associated with diverse cellular activities) protease known for degrading poorly folded and damaged proteins and is often classified as a weak protein unfoldase. Here, using a Lon-degron pair from *Mesoplasma florum* (*Mf*Lon and *Mf*ssrA, respectively), we perform ensemble and single-molecule experiments to elucidate the molecular mechanisms underpinning *Mf*Lon function. Notably, we find that *Mf*Lon unfolds and degrades stably folded substrates and that translocation of these unfolded polypeptides occurs with a ~6-amino-acid step size. Moreover, the time required to hydrolyze one ATP corresponds to the dwell time between steps, indicating that one step occurs per ATP-hydrolysis-fueled "power stroke." Comparison of *Mf*Lon to related AAA+ enzymes now provides strong evidence that HCLR-clade enzymes function using a shared power-stroke mechanism and, surprisingly, that *Mf*Lon is more processive than ClpXP and ClpAP. We propose that ample unfoldase strength and substantial processivity are features that contribute to the Lon family's evolutionary success.

INTRODUCTION

Proteolysis eliminates proteins that are unfolded, misfolded, or permanently damaged due to heat, chemical, oxidative, or nutritional stresses. In addition to this important role in protein quality control (pQC), proteolysis is critical for adjusting the proteome by removing proteins that are no longer needed or that serve regulatory roles, especially as cells respond to environmental stimuli and enter new growth and development stages. In bacteria, a group of proteases of the AAA+ (ATPases associated with diverse cellular activities) family degrade protein substrates in the cytoplasm and inner membrane. A hexameric ring-shaped AAA+ unfoldase module in these enzymes uses energy from ATP hydrolysis to denature and translocate substrates into a compartmentalized proteolytic chamber (Figure 1A). AAA+ proteases typically recognize target substrates by binding to a specific peptide degradation tag (degron) or, in some cases, by interacting with less well-defined recognition features.[1–5]

Substrate degrons often initially interact with pore loops within the axial channel of the AAA+ ring.[6–10] Movement of these pore loops via a "power stroke" that requires ATP hydrolysis can then pull on the native portion of the substrate and thus exert a mechanical unfolding force. A power stroke coinciding with thermal fluctuations that transiently destabilize the native substrate is likely to be the key event leading to cooperative mechanical unfolding of most proteins or their component domains.[11–13] However, depending on the force applied and the stability of the native structure, many unsuccessful power strokes may occur before unfolding. Following substrate unfolding, additional power strokes translocate the denatured polypeptide through the axial channel and into the peptidase chamber for degradation into short peptides.

There is substantial interest in elucidating how the energy from ATP hydrolysis by AAA+ unfoldases is transmitted to the pore loops and, in turn, how they pull on and translocate the substrate polypeptide in the central channel. A structure-inspired model where ATP hydrolysis by each subunit moves the substrate through the channel in two-amino-acid steps is popular based on cryoelectron microscopy (cryo-EM) structures of substrate-bound AAA+ enzymes with their pore loops spaced every two residues along the substrate. However, biophysical studies of translocation step sizes, single-molecule experiments, and active/inactive subunit-mixing assays do not fit this model and thus necessitate consideration of alternative mechanisms.

The AAA+ Lon protease is present in most bacteria and organelles of bacterial origin in many eukaryotic cells. In the bacterial genus Mycoplasma, including *Mesoplasma florum*, which has undergone extensive genome minimization, Lon is the only soluble cytoplasmic AAA+ protease, whereas it is joined by ClpXP, ClpAP, and HslUV in *Escherichia coli*. *E. coli* Lon has a major pQC role and is estimated to degrade at least half of the proteome when proteins are truncated or contain amino acid analogs,

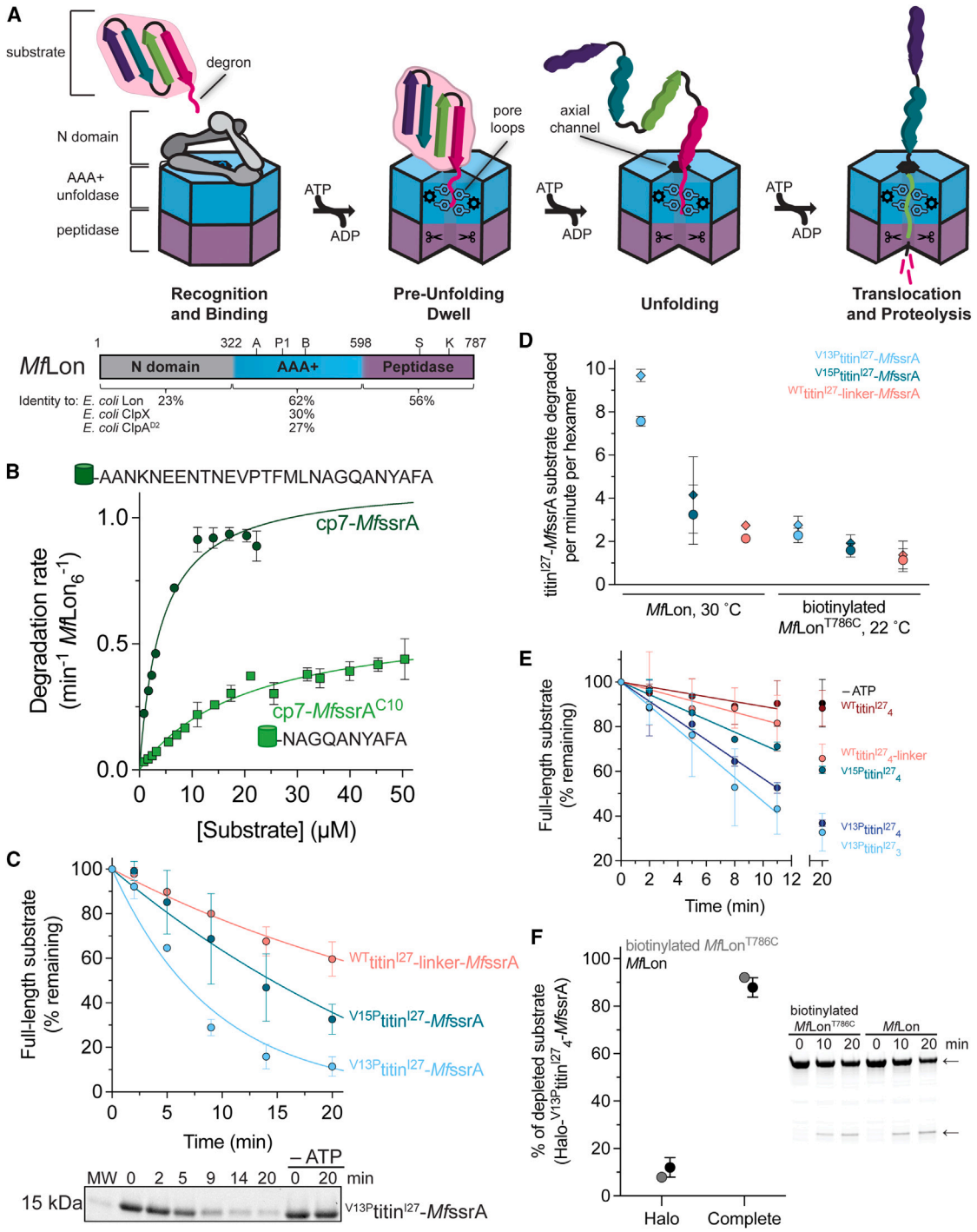

Figure 1. *Mf*Lon efficiently degraded *Mf*ssrA-tagged proteins of different stabilities

(A) Overview of AAA+ protease structure and mechanism with Lon as the example enzyme (top). Amino acid sequence identity (%) of *Mf*Lon compared with *E. coli* Lon, ClpX, and ClpA^{D2}. A, B, and P1 show the approximate locations of the Walker-A and -B motifs and the P1 loop of the ATPase, respectively. S and K mark the catalytic serine and lysine of the peptidase domain.

(B) Michaelis-Menten fits for degradation of cp7 with two *Mf*ssrA degrons. Compared with the truncated degron (*Mf*ssrA^{C10}), the full-length *Mf*ssrA degron promoted faster degradation (V_{max} = 1.1 ± 0.1 min^{-1} hexamer^{-1}) and had a lower Michaelis constant (K_M = 4.2 ± 0.6 μM). For cp7-*Mf*ssrA^{C10}, V_{max} = 0.61 ± 0.04 min^{-1} hexamer^{-1} and K_M = 20.6 ± 3 μM. Rates are averages ± 1 SEM of three independent measurements.

(C) Degradation rates of single-domain titin^{I27}-*Mf*ssrA variants correlate with substrate stability. Assays were done with 15 μM substrate, 150 nM *Mf*Lon$_6$, and 5 mM ATP. Values are averages ± 1 SD of three independent measurements, and curves were fit to single-exponential decay functions. A representative

(legend continued on next page)

often by recognizing short stretches of hydrophobic residues that become exposed when proteins fail to fold or unfold due to environmental stress.[3,14] *E. coli* Lon also degrades regulatory proteins, such as SulA.[15,16] Unfortunately, no high-affinity degron has yet been identified for *E. coli* Lon, which has hampered biophysical studies. In Mycoplasma, however, Lon recognizes and degrades proteins bearing the ssrA degron with a K_M of ~3–5 μM (Table S1).[17,18] Here, we use *Mesoplasma florum* Lon (*Mf*Lon) to conduct ensemble degradation and ATPase assays and single-molecule optical trapping analysis of protein unfolding and translocation to dissect the enzymatic and mechanical features of Lon degradation.

We find that *Mf*Lon can degrade stable model proteins such as degron-tagged GFP and, as expected based on earlier work, the titin^{I27} domain.[17] Optical trapping demonstrates that *Mf*Lon requires longer times to unfold stable protein domains compared to *E. coli* ClpXP or ClpAP, yet it has a higher probability of processively and completely degrading a multi-domain substrate than these enzymes.[11,19,20] Moreover, although Lon's average translocation velocity is slower, it takes individual steps of a size (1 nm or 4–8 residues) similar to ClpXP and ClpAP while hydrolyzing approximately one ATP per step. These results contrast with predictions of the structure-inspired "two-residue step" translocation model and strongly support the conclusion that HCLR-clade, named after the main family members HslU/Clp/Lon/RuvB, AAA+ proteases employ a conserved mechanism of transforming the energy of ATP hydrolysis into mechanical work.

RESULTS

Lon degrades very stable substrates in ensemble assays

To quantify and compare *Mf*Lon's ability to degrade substrates with different characteristics, we first established standard assay conditions. ATPase kinetics and degradation assays using fluorescein isothiocyanate (FITC)-casein, a molten-globule substrate, revealed that *Mf*Lon was most active at lower hexamer concentrations (~50–150 nM) (Figures S1A and S1B), and these concentrations were used for later experiments. Next, to determine which variant of the *M. florum* ssrA (*Mf*ssrA) degron directs degradation most effectively,[17] we constructed two substrates using the model protein cp7-^{SF}GFP (called cp7 hereafter), which is a circularly permuted green fluorescent protein that is easier to unfold than the unpermuted protein.[21,22] These proteins carried at their C termini either the 27-residue, full-length *Mf*ssrA degron (generating cp7-*Mf*ssrA) or a truncated degron containing only the C-terminal ten residues (*Mf*ssrA^{C10}, generating cp7-*Mf*ssrA^{C10}).[17] The degrons were added by sortase ligation to avoid substantial nonspecific proteolysis of the extended, unstructured C-terminal segment during overexpression and purification (see STAR Methods; sequences of degrons in Tables S1 and S2). *Mf*Lon degraded both cp7-*Mf*ssrA and cp7-*Mf*ssrA^{C10}, but Michaelis-Menten analysis revealed that the K_M was about 5-fold smaller and the V_{max} was about 1.5-fold faster for cp7-*Mf*ssrA degradation (Figure 1B). Given that a smaller K_M is generally important for the success of single-molecule experiments, the wild-type *Mf*ssrA degron was used in all subsequent experiments, including for the optical trapping described below.

To systematically interrogate *Mf*Lon's activity against protein substrates of differing stabilities, we appended the *Mf*ssrA degron to the wild-type (WT) titin^{I27} domain, the mildly destabilized ^{V15P}titin^{I27} mutant, or the highly destabilized ^{V13P}titin^{I27} mutant (Table S2). The V13P and V15P mutations reduce both the global thermodynamic and the mechanical stability of the titin^{I27} domain.[11,23–25] As assayed by SDS-PAGE, *Mf*Lon degraded ^{V13P}titin^{I27}-*Mf*ssrA about twice as fast as ^{V15P}titin^{I27}-*Mf*ssrA (Figure 1C) but did not detectably degrade ^{WT}titin^{I27}-*Mf*ssrA. However, when an 11-residue linker was inserted adjacent to the degron (generating ^{WT}titin^{I27}-linker-*Mf*ssrA), *Mf*Lon was able to degrade the very stable ^{WT}titin^{I27} domain, albeit slowly (Figure 1C; Table S2).

Under physiological conditions, the faster-maturing mut3 variant of GFP (which contains the mutations S65G and S72A) spontaneously denatures with a half-life of ~20 years, and given that degron-tagged GFP variants can be degraded by ClpXP and ClpAP in minutes, these AAA+ proteases enhance the rate of GFP unfolding by ~10^7-fold.[19,25–27] We found that *Mf*Lon degraded degron-tagged GFPmut3 fastest with a linker-*Mf*ssrA degron, slower with an *Mf*ssrA degron, and slowest with an *Mf*ssrA^{C10} degron (Figure S1C). Thus, like other AAA+ proteases, *Mf*Lon catalyzes unfolding and degradation of very stable protein substrates.

Single-molecule optical trapping

The design of our optical-trapping assay is depicted in Figure 2A. *Mf*Lon^{T786C}, ~30% biotinylated with maleimide-PEG$_2$-biotin at Cys^{786}, is attached to a streptavidin-coated microscope slide. A multi-domain substrate is tethered, via a double-stranded 1,010-bp DNA linker, to a 1.09 μm anti-digoxigenin-coated bead. This functionalized laser-trapped bead is scanned along the surface until engagement of the substrate by surface-tethered

SDS-PAGE gel, stained with Coomassie blue, shows degradation of ^{V13P}titin^{I27}-*Mf*ssrA (13.9 kDa) by *Mf*Lon. Control samples lacking ATP were taken at the start and end of the experiment.

(D) Comparison of degradation rates by *Mf*Lon at 30°C and biotinylated *Mf*Lon^{T786C} at 22°C. Initial degradation rates (circles, min^{-1} hexamer^{-1}) were determined with 0.15 μM *Mf*Lon and 20 μM titin^{I27} or 0.45 μM biotinylated *Mf*Lon^{T786C} and 15 μM titin^{I27}. Calculated V_{max} rates (diamonds, min^{-1} hexamer^{-1}) were determined by dividing the initial rate by the fractional saturation (K_M = 4.2 μM). Values are averages ± 1 SEM of three independent measurements.

(E) Rates of degradation of multi-domain substrates at 30°C correlated with substrate stability. Values are averages ± 1 SD of three independent measurements, and curves were fit to single-exponential decay functions. Degradation assays were conducted with 3 μM of the multi-domain substrates, 150 nM *Mf*Lon$_6$, and 5 mM ATP.

(F) Ensemble degradation of Halo-^{V13P}titin$^{I27}_4$-*Mf*ssrA (top arrow) by *Mf*Lon and biotinylated *Mf*Lon^{T786C} at 22°C. Assays were done with 3 μM substrate and 150 nM hexamer enzyme. Values are averages ± 1 SD of three independent measurements. *Mf*Lon depleted ~50% and biotinylated *Mf*Lon^{T786C} depleted ~45% of the starting substrate after 20 min. For both enzymes, 88%–92% of the depleted substrate was fully degraded, and the remaining ~8%–12% accumulated as a fragment containing the Halo domain (bottom arrow).

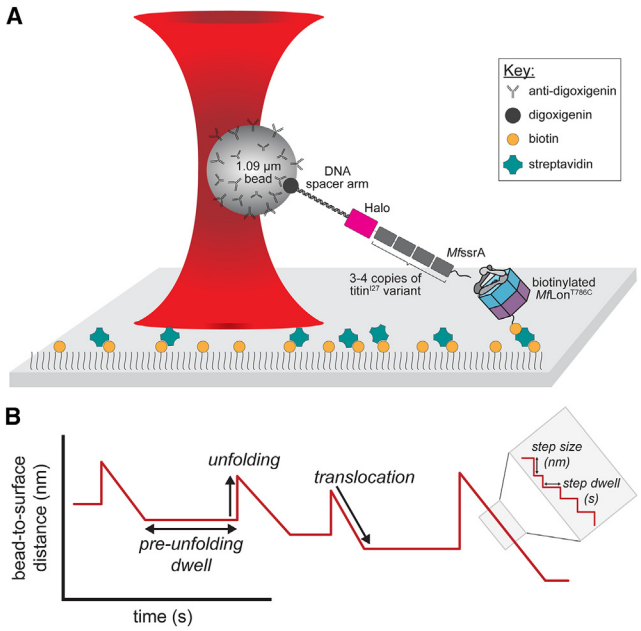

Figure 2. Experimental design of single-molecule optical trapping by *Mf*Lon

(A) Cartoon representation of the single-laser, single-bead optical trap setup. (B) Schematic of single-molecule traces for degradation of a multi-domain substrate.

*Mf*Lon. Unfolding and translocation of the substrate is then assayed via changes in the position of the bead in the laser, which depends on the distance between surface-bound *Mf*Lon and the bead. Unfolding of a substrate domain triggers a very rapid increase in this distance, whereas subsequent stepwise translocation of the polypeptide results in a gradual decrease in distance with time (Figure 2B). Pre-unfolding dwells (PUDs) are intervals during which *Mf*Lon unsuccessfully attempts to unfold a domain of the substrate, and thus the bead-to-enzyme distance does not change (Figure 2B). Our assay is similar to the dual-bead "dumbbell" setup used to measure unfolding and translocation of similar multi-domain substrates by *E. coli* ClpXP and ClpAP.[12,19,20,25,28,29]

Due to the temperature dependence of *Mf*Lon activity, we used ensemble assays to compare the degradation rate of the three titin^{I27} variants by WT *Mf*Lon at 30°C, where it is maximally active,[17] and biotinylated *Mf*Lon^{T786C} at 22°C, the temperature at which optical-trapping experiments were performed (Figure 1D). Initial degradation rates were determined at subsaturating concentrations of substrate, from which a lower bound on V_{max} values were calculated (Figure 1D). At 22°C, degradation was substantially slower but exhibited the same general dependence on substrate stability as observed at 30°C.

For our single-molecule experiments, we used three different multi-domain substrates, each with (1) an N-terminal Halo domain to link the protein to DNA, (2) three or four copies of ^{WT}titin^{I27}, ^{V15P}titin^{I27}, or ^{V13P}titin^{I27}, and (3) a C-terminal *Mf*ssrA or linker-*Mf*ssrA degron (Table S2). *Mf*Lon degradation of these multi-domain substrates was verified in ensemble assays (Figure 1E), with faster degradation observed for the destabilized titin^{I27} variants. Control degradation assays confirmed that biotinylated *Mf*Lon^{T786C} had degradation activity similar to WT *Mf*Lon (Figure 1F).

Optical trap distance versus time traces for *Mf*Lon degradation of each substrate were collected (n = 57 for Halo-^{V13P}titin$^{I27}_3$-*Mf*ssrA; n = 47 for Halo-^{V15P}titin$^{I27}_4$-*Mf*ssrA; and n = 14 for Halo-^{WT}titin$^{I27}_4$-linker-*Mf*ssrA). One difference between dual-trap and single-trap experiments is that the former can be performed in a regime where the average force does not change during the measurement (see the supplemental information for an explanation of differences between instrument and enzyme forces).[30] In the single-trap experiment, the force changes with motion, but the range of forces experienced by the substrate during our experiments (between 0.1 and 22 pN) overlapped those in dual-trap studies (Figures S2D and S4).[12,19,20,25] To allow direct comparison, we collected several trajectories for *Mf*Lon degradation of Halo-^{V13P}titin$^{I27}_3$-*Mf*ssrA (n = 14) using a dual-trap instrument and found general agreement with results from the single-trap assay (Figures S2A–S2C). Importantly, however, enzyme-substrate tethers formed reliably with the single-bead setup but only occasionally in the dual-bead assay.

PUD times depend on domain stability

Representative single-molecule trajectories are shown in Figure 3A for *Mf*Lon degradation of the *Mf*ssrA-tagged multi-domain substrates ^{V13P}titin$^{I27}_3$ (Figures 3Ai–3Aiii), ^{V15P}titin$^{I27}_4$ (Figures 3Aiv–3Avi), and ^{WT}titin$^{I27}_4$-linker (Figures 3Avii–3Aix). Each trace contained at least one titin^{I27} unfolding event, and several also recorded unfolding of the Halo domain (pink), which results in a larger extension because of the size of Halo (311 residues) compared to titin^{I27} (89 residues). In most cases, unfolding was rapid and highly cooperative, although we occasionally observed a titin^{I27} unfolding intermediate (see trace iii, unfolding event two), which has been detected and characterized previously.[20] Each unfolding event was followed by a translocation run whose length was consistent with the expected value for translocation of a fully unfolded domain.

Most traces with multiple unfolding events showed a distinct PUD time after completion of each translocation phase. As initially described for ClpXP experiments,[12] we interpret these dwells to reflect the time during which the AAA+ unfoldase carries out multiple ATP-dependent power strokes that fail to unfold the engaged domain. As shown in Figure 3B, the lengths of the PUDs for the ^{V13P}titin^{I27} and ^{V15P}titin^{I27} variants were roughly exponentially distributed with an average time that was fastest for the less stable ^{V13P}titin^{I27} domain ($\tau \sim 8$ s; n = 67) and longer for the more stable ^{V15P}titin^{I27} domain ($\tau \sim 20$ s; n = 82). Bootstrap resampling confirmed that the mean PUDs for ^{V13P}titin^{I27} and ^{V15P}titin^{I27} were statistically distinct (Table S3). Only 13 PUDs were recorded for the ^{WT}titin^{I27} domain, and analysis of just these limited data gave an unexpectedly short average unfolding time ($\tau \sim 13$ s), which we reasoned was likely due to biased sampling (Figures S3C and S3D). Therefore, we instead focused on the initial dwells, defined as the time between the start of the trace and the first unfolding event. The initial dwell can only be as long as or shorter than a true internal PUD given that data

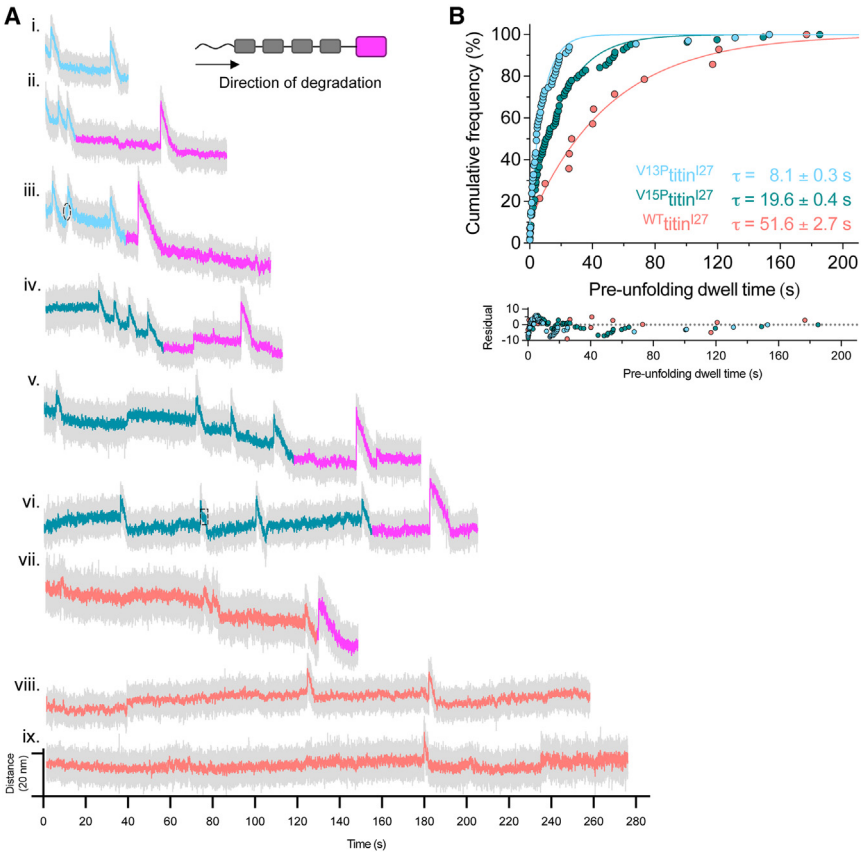

Figure 3. PUD times vary within a single trace and between traces

(A) Example single-molecule traces for degradation of Halo-^{V13P}titin$^{I27}_3$ (i–iii), Halo-^{V15P}titin$^{I27}_4$ (iv–vi), and Halo-^{WT}titin$^{I27}_4$-linker (vii–ix). Traces are shown with the raw data (gray, 3,000 Hz) overlaid by the decimated averaged data (50 Hz) colored by the identity of the protein domain (blue: ^{V13P}titin^{I27}, teal: ^{V15P}titin^{I27}, orange: ^{WT}titin$^{I27}_4$, pink: Halo). Circled: intermediate in unfolding. Boxed: pause during translocation. Trace (ix) had a perturbation in the flow cell, causing a signal shift and increased noise at the end of the final dwell. Some of the traces had extended dwells between the end of Halo translocation and rupture of the tether, which were truncated for clarity. Due to the surface-coupling assay setup, drift of the sample plane was recorded in some traces with the baseline of the trace moving at a gradual and generally uniform rate due to continual bead movement in the x, y, or z direction (e.g., traces iii and vii).

(B) PUD times for titin^{I27} variants. ^{V13P}titin^{I27} dwells (n = 67) were shorter than ^{V15P}titin^{I27} dwells (n = 82), which were intermediate in time compared with ^{WT}titin^{I27} initial unfolding dwells (n = 14). Because there were very few traces for Halo-^{WT}titin$^{I27}_4$-linker, the data for the ^{WT}titin^{I27} dwell calculation was from the time constant of the initial dwell (Figure S3).

collection may not start as soon as the enzyme-substrate tether forms. For ^{V13P}titin^{I27} and ^{V15P}titin^{I27}, the distributions of these initial dwells were approximately the same as the PUD distribution (Figures S3A, S3B, and S3D); thus, we reasoned that the initial dwells would represent a meaningful lower-threshold value for the true PUD for the ^{WT}titin^{I27} domain, and an exponential fit of these initial dwells gave an unfolding time of $\tau \sim 52$ s (n = 14) (Figure 3B, S3C, and S3D; Table S3). PUDs for *Mf*Lon unfolding of the Halo domain (n = 50) were exponentially distributed with an average of ~28 s, suggesting that this protein is intermediate between the ^{V15P}titin^{I27} and ^{WT}titin^{I27} domains in its resistance to enzymatic unfolding (Table S3; Figure S3E).

Translocation velocity and stepping

Following unfolding of ^{V13P}titin^{I27}, ^{V15P}titin^{I27}, or ^{WT}titin^{I27} domains by *Mf*Lon, the average rate of translocation was determined by dividing the length of the polypeptide chain translocated by the total translocation time. The translocation rates for all three titin^{I27} domains were within error (combined rate of 3.4 ± 0.1 nm s^{-1}), as expected given that these sequences differ only by a single amino acid (Table S4; see Figure S4A for more details). Because the Halo domain contains a covalent link to the DNA handle, we did not analyze its translocation.

Translocation is composed of distinct steps that reflect fundamental characteristics of the mechanism of enzyme movement. Previously, multiple step-finding algorithms were tested for *E. coli* ClpXP and ClpAP translocation, and the chi-squared minimization method[31] was deemed best for fitting data with rapid, small, and irregular steps.[12,19,20,25] Representative fits of four *Mf*Lon translocation runs using this method are shown in Figure 4A. For the three stability variants of titin^{I27}, we found no difference in stepping characteristics, and thus these datasets were pooled (n = 2,449 total steps). As described previously,[19,25] a minimum detectable step-size threshold was set to 0.75 nm such that all smaller or backward steps were combined until this threshold was met. However, because this threshold is close to our observed most abundant step size, we also performed the analysis using a 0.5-nm threshold to determine if the larger threshold was biasing the detection against smaller steps. We found that both sets of step fits were in general agreement (Figure S5). Moreover, the distributions of step sizes and step dwells were similar (Figures S5A–S5C), although the average step size and step dwell time were slightly smaller due to the addition of ~1.5 steps per translocation on average (Figure S5D). Importantly, however, the most probable step size remained the same (Figure S5A), and the number of amino acids translocated per nm was also unchanged (Figure S5D). Through visual interrogation of representative traces, it appears that about half of the additional steps generated with the 0.5-nm threshold resulted in overfitting of the data, placing a step where none was visible (Figure S5E). Overall, these analyses suggest that the use of the 0.75-nm threshold for the step-fitting analysis does not omit many smaller steps.

Figure 4B illustrates a summary of the step-size results using the 0.75-nm threshold. *Mf*Lon took physical steps ranging from

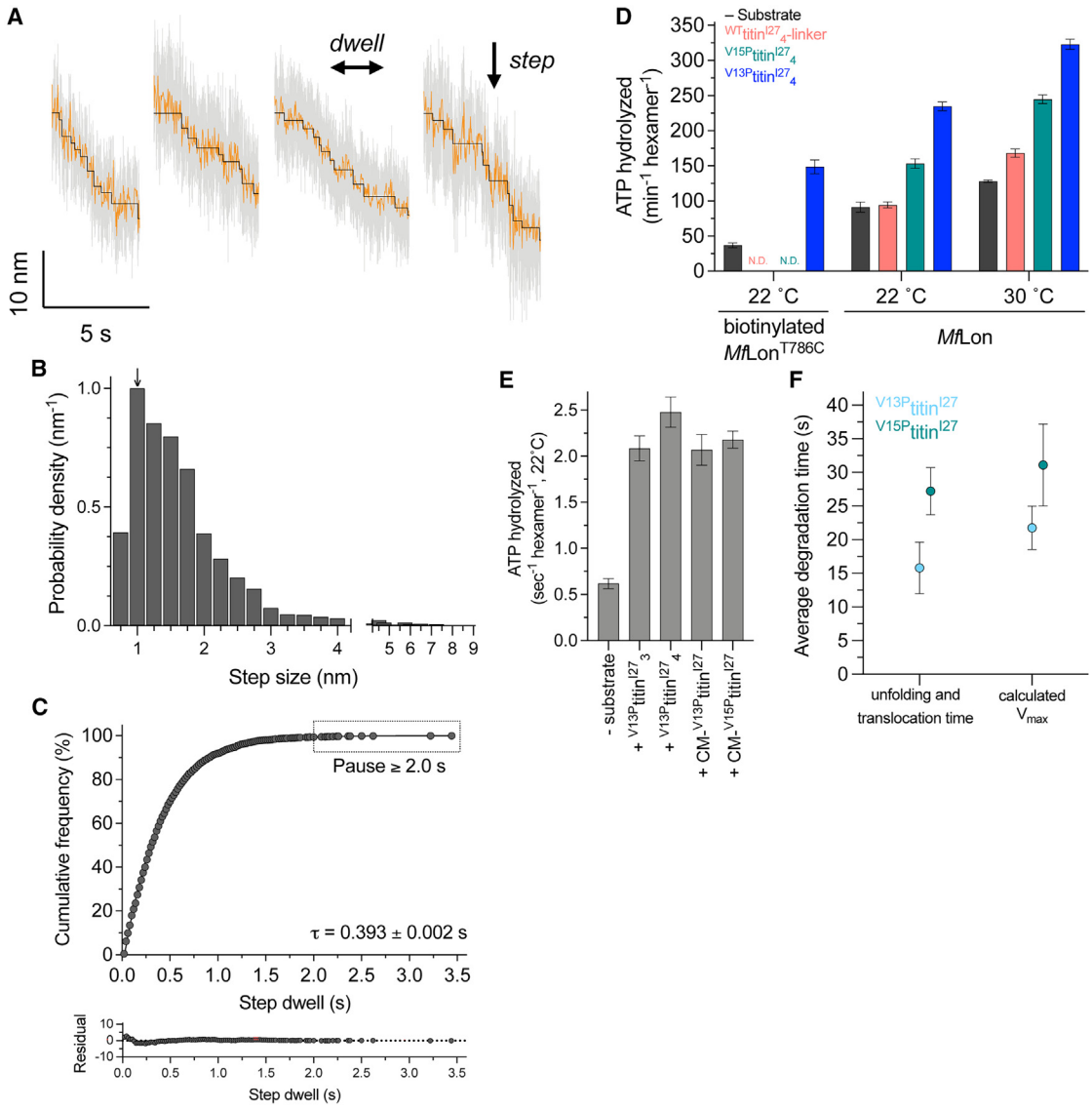

Figure 4. Translocation and stepping characteristics of *Mf*Lon

(A) Representative titin^{I27} translocations with step fits. The raw data (3,000 Hz, gray) was decimated and calculated with a 10-point moving average to 50 Hz (orange), and steps (black) were fit using a chi-squared minimization method (see STAR Methods).

(B) Histogram of step sizes. All titin^{I27} translocations (n = 2,449) were combined and fit by chi-squared minimization to determine step sizes in nm. The minimum step size threshold was set to 0.75 nm, as described.[25] The arrow indicates the most abundant step size of 1 nm.

(C) Distribution of step dwells. All titin^{I27} translocations were combined and fit by chi-squared minimization to determine step dwells (n = 2,296). The smallest detectable step dwell is 0.02 s (50 Hz). The single-exponential fit gives a time constant of ~0.39 s. A step dwell of 2 s or longer was considered a pause.

(D) ATP-hydrolysis rates for *Mf*Lon and biotinylated *Mf*Lon^{T786C}. The ATPase rates were temperature dependent and stimulated to a lesser degree by more stable protein substrates. *Mf*Lon hydrolyzes ATP more slowly in the absence of substrate. Values are averages ± 1 SEM of three independent measurements.

(E) ATP hydrolysis rate per second of biotinylated *Mf*Lon^{T786C} at 22°C. The ATPase rate in the absence of substrate was 37 ± 3 ATP min^{-1} hexamer^{-1} but was stimulated to 125 ± 18 and 149 ± 10 ATP min^{-1} hexamer^{-1} in the presence of an excess of ^{V13P}titin$^{I27}_3$ or ^{V13P}titin$^{I27}_4$ (16 μM), respectively. The concentrations of CM-^{V13P}titin^{I27} and CM-^{V15P}titin^{I27} were 8 and 28 μM, respectively. Values are averages ± 1 SEM of three independent measurements.

(F) Average degradation time for a single titin^{I27} domain as determined in single-molecule and ensemble experiments. For the single-molecule data, n = 52 for ^{V13P}titin^{I27} and n = 82 for ^{V15P}titin^{I27}. Ensemble values are averages ± 1 SEM of three independent measurements.

0.75 to 8.9 nm in length, with the most abundant step size being 1 nm and the average step size being 1.66 ± 0.02 nm (Figure 4B). The difference in these values arose because the step distribution was asymmetric, with a shoulder composed of longer steps. Approximately ~80% of steps were 2 nm or smaller and 95% were 3 nm or smaller; hence, most events could consist of ~1-nm steps, with two or three of these steps sometimes occurring too rapidly to be separated. There was no clear

pattern to the order of 1- and 2-nm steps: the probability of a 1-nm step was greatest regardless of whether the preceding or following step(s) was 1 or 2 nm in length (Figure S6). Overall, these results indicate that *Mf*Lon translocates polypeptides principally using a fundamental step of ~1 nm.

Step dwell time is similar to the time required to hydrolyze one ATP

Each translocation step is preceded by a step dwell (n = 2,296), a value determined during chi-squared minimization step fitting. For *Mf*Lon, step dwells ranged from 0.02 (the lower threshold of detection for the 50 Hz decimated and averaged data) to 3.4 s. The cumulative distribution of step dwells fit to a single-exponential function with $\tau = 0.393 \pm 0.002$ s (Figure 4C). Translocation-step dwells of 2 s or longer were considered pauses, defined as a time ~5-fold longer than the average step dwell time,[20] and occurred in roughly 0.6% of total *Mf*Lon steps.

To test if the translocation-step dwells were similar to the time required to hydrolyze ATP, we determined the ATP-hydrolysis rate of *Mf*Lon and biotinylated *Mf*Lon^{T786C} under conditions closely mimicking those in the trap. Notably, the ATPase activity of biotinylated *Mf*Lon^{T786C} was suppressed compared with the native enzyme (Figure 4D). The rate of *Mf*Lon ATP hydrolysis also depended on temperature and could be stimulated by as much as ~2.5-fold when bound by a protein substrate (Figure 4D). Interestingly, we observed the highest level of substrate stimulation for the multi-domain ^{V13P}titin^{I27} variant, followed by the ^{V15P}titin^{I27} and then the ^{WT}titin^{I27} substrates (Figure 4D). As length of the PUDs show a strong dependence on substrate stability, whereas translocation rates and step dwells do not (Figure S4), we posit that *Mf*Lon has a slower ATPase rate during attempted unfolding and a faster rate during translocation, as suggested in studies of ClpXP degradation.[11]

In the presence of a high concentration of the multi-domain ^{V13P}titin^{I27} substrate at the temperature used for optical trapping (22°C), the biotinylated *Mf*Lon^{T786C} hexamer hydrolyzed one ATP in ~0.4–0.5 s (Figure 4E). Because this rate includes hydrolysis rates during unfolding and translocation, we also carboxymethylated (CM) the cysteines in the ^{V13P}titin^{I27} substrate, which results in domain unfolding,[11,32] and retested ATP hydrolysis. The ATPase rate for CM-^{V13P}titin^{I27} was within error of the rate with the corresponding native substrate (Figure 4E). Importantly, the ensemble ATP hydrolysis rate (~0.4–0.5 s) and the average step dwell time (~0.43 s) are very similar, suggesting that each translocation step corresponds to movement fueled by hydrolysis of one ATP.

Moreover, to determine if the single-molecule and ensemble assays measure similar degradation rates for *Mf*Lon, we compared the average time for degradation of single titin^{I27} domains in both assays (Figure 4F). By averaging the times for the PUD plus subsequent translocation, we determined the average degradation times in the optical trap to be ~16 s for ^{V13P}titin^{I27} and ~27 s for ^{V15P}titin^{I27} (degradation time was not determined for the ^{WT}titin^{I27} substrate). The calculated V_{max} values from the ensemble experiments yielded average degradation times of ~22 s for ^{V13P}titin^{I27} and ~31 s for ^{V15P}titin^{I27} (Figure 1D). The time required for degradation in ensemble assays includes initiation steps (i.e., degron recognition, substrate engagement, etc.) that are not captured in the optical trap. Therefore, as expected, the average degradation time was slightly longer in the ensemble experiments; nonetheless, these values were within error of the average single-molecule degradation times. Thus, we conclude that these two distinct types of data agree well and capture important parameters of degradation by *Mf*Lon.

*Mf*Lon is highly processive

Our ensemble and single-molecule experiments show that *Mf*Lon is highly processive, defined as the ability to degrade successive domains in engineered substrates before losing grip and terminating degradation. For example, as shown in Figure 5A, after eliminating traces with just one unfolding event, at least half of the remaining traces of ^{V13P}titin^{I27} and ^{V15P}titin^{I27} degradation contained a Halo unfolding extension (~55% for ^{V13P}titin^{I27} [n = 42]; 50% for ^{V15P}titin^{I27} [n = 40]), demonstrating that *Mf*Lon had already degraded either three ^{V13P}titin^{I27} domains or four ^{V15P}titin^{I27} domains. Due to assay setup time, early unfolding events are often missed, but Halo domain degradation can only occur after the unfolding and translocation of the titin^{I27} domains. These data provide evidence that *Mf*Lon degrades these substrates with a high degree of processivity. In fact, ~30% of the traces contained all four (Halo-^{V13P}titin$^{I27}{}_3$) or five (Halo-^{V15P}titin$^{I27}{}_4$) unfolding events, directly demonstrating that the entire substrate was degraded. Traces that did not contain a Halo unfolding event had no obvious pattern of premature dissociation products, although the most abundant class of traces had two titin^{I27} unfolding events for both the ^{V13P}titin^{I27} and ^{V15P}titin^{I27} substrates (Figure 5A). Thus, these results indicate that *Mf*Lon is both a "strong" enough unfoldase and a processive enough translocase to successfully degrade a protein containing five meta-stable to moderately stable domains and a total of 720 amino acids. For *Mf*Lon degradation of the more stable multi-domain substrate containing ^{WT}titin^{I27}, 2 of 14 traces contained a Halo unfolding event (Figure 5A), indicating successful unfolding and degradation of four ^{WT}titin^{I27} domains.

Following covalent modification of the Halo domain with a fluorescent ligand, we monitored degradation of the multi-domain substrates after SDS-PAGE by fluorescence. To assess processivity, we first calculated the fraction of substrate that had been degraded to some extent (based on loss of the intact substrate band) and then the percentage of the degraded protein that appeared in specific truncation products. For Halo-^{V13P}titin$^{I27}{}_4$-*Mf*ssrA and Halo-^{V15P}titin$^{I27}{}_4$-*Mf*ssrA, degradation was fast and efficient at 30°C, and no intermediates or truncation products accumulated except for minor appearance of a band (~5% of the depleted substrate) corresponding to a single Halo domain (Figures 5B and S7). Hence, once *Mf*Lon initiates degradation of these substrates, it completes proteolysis of the entire substrate >90%–95% of the time. During degradation of Halo-^{WT}titin$^{I27}{}_4$-linker-*Mf*ssrA substrate, however, there was some accumulation of partially-degraded products (Figure 5B). The apparent molecular weights of these products indicated that *Mf*Lon stalls or disassociates principally when trying to unfold a ^{WT}titin^{I27} domain. We also assayed degradation of Halo-^{WT}titin$^{I27}{}_4$-linker-*Mf*ssrA at 22°C and observed more accumulation of partially degraded species, but there was still

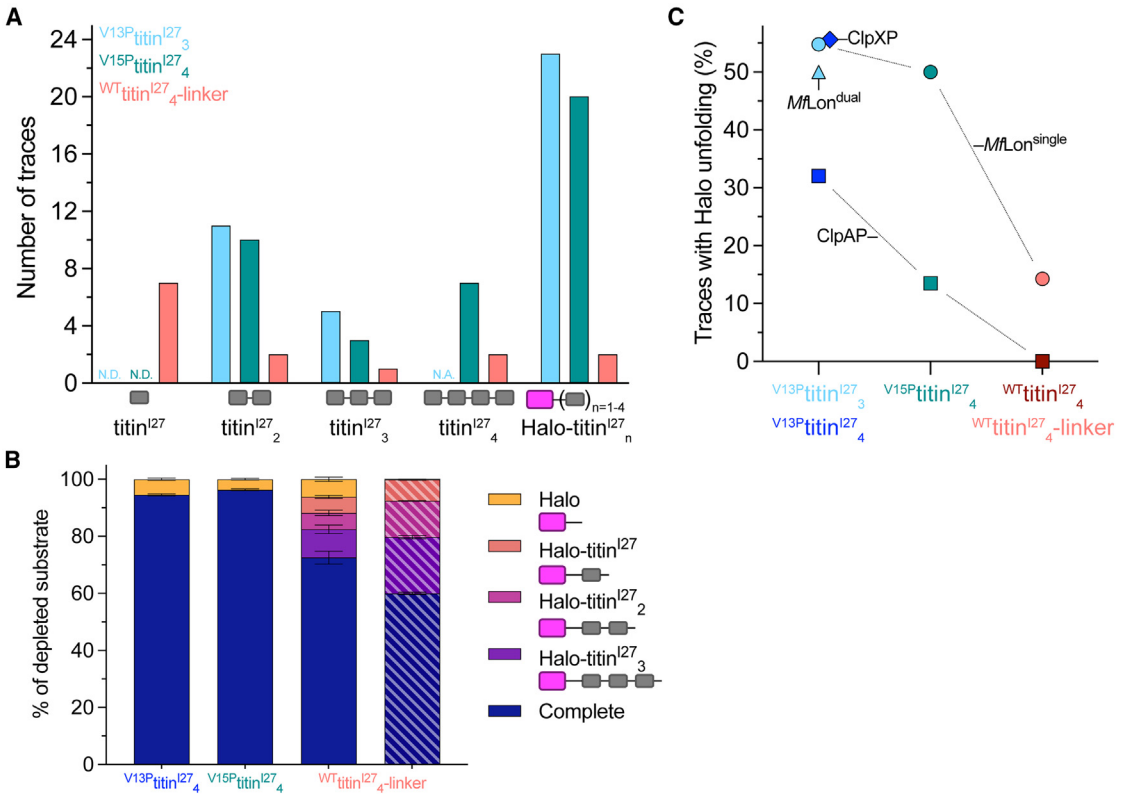

Figure 5. *Mf*Lon is highly processive during degradation of both destabilized and highly stable multi-domain substrates in single-molecule and ensemble assays

(A) Single-molecule traces of all titin^{I27} variants had a reasonably high probability of containing a Halo unfolding event. For the Halo-^{V13P}titin$^{I27}_3$ and Halo-^{V15P}titin$^{I27}_4$ substrates, traces with only one unfolding event were discarded. Because of the slow unfolding of ^{WT}titin^{I27} and the low number of traces, we included the traces with just one unfolding event because the likelihood that it corresponded to titin^{I27} unfolding was high. Plotted in groups are the number of domains observed in the single-molecule traces with each substrate.

(B) Ensemble assays revealed complete degradation of most of the engaged multi-domain substrates. Accumulation of partially degraded truncation products was negligible for Halo-^{V13P}titin$^{I27}_4$ and Halo-^{V15P}titin$^{I27}_4$ at 30°C except for a low level of Halo domain accumulation (yellow). For Halo-^{WT}titin$^{I27}_4$-linker, significant accumulation of truncations occurred both at 30°C (solid) and 22°C (striped), but most of the engaged substrate was still fully degraded (~60%–70%). Accumulation of the Halo domain at 22°C was minor (<1%) and near the limit of detection. Values are averages ± 1 SEM of three independent measurements. Cartoons on the right are schematic representations of the four distinct truncation products.

(C) *Mf*Lon has a much higher probability of complete degradation of multi-domain substrates compared to ClpAP. For *Mf*Lon, 23 of 42 ^{V13P}titin$^{I27}_3$ traces, 20 of 40 ^{V15P}titin$^{I27}_4$ traces, and 2 of 7 ^{WT}titin$^{I27}_4$-linker traces contained a Halo unfolding event. For ClpAP, 16 of 50 ^{V13P}titin$^{I27}_4$ traces and 10 of 74 ^{V15P}titin$^{I27}_4$ traces contained a Halo unfolding event. ClpAP did not degrade ^{WT}titin$^{I27}_4$ in single-molecule assays. There is no available single-molecule data for the comparison of ClpXP degradation of the ^{V15P}titin$^{I27}_4$ or ^{WT}titin$^{I27}_4$ substrates. ClpAP data were calculated from data presented by Olivares et al.[19] and Kotamarthi et al.[20] Data points are offset for clarity.

complete processing of ~60%–70% of the substrates on which degradation had been initiated (Figure 5B). As inferred from the single-molecule traces, these data reveal that *Mf*Lon can often processively unfold and then translocate a protein with four adjacent WT titin^{I27} domains, albeit with less success at lower temperatures. We conclude that *Mf*Lon is a tenacious unfoldase and translocase that is likely to completely degrade any protein that it successfully engages (see Figure 5C and discussion).

DISCUSSION

As most bacteria, mitochondria, and chloroplasts use several different AAA+ proteases, the features that distinguish these enzymes and the advantages of having multiple family members are being actively investigated. Distinguishing characteristics include substrate specificity, enzyme architecture, ATPase rates, and mechanical unfolding strengths. Among the five common AAA+ proteases in bacteria, Lon is the most widely distributed cytoplasmic enzyme, yet features of Lon that explain its "evolutionary success" are unclear. For example, Lon's reported weak unfolding ability is a property that might seem to limit widespread efficacy.[33] However, analysis of Lon mechanics has been hampered by lack of a high-affinity degron that converts model proteins into substrates. Our use of the *M. florum* Lon/ssrA pair solved this issue and allowed us to characterize unfoldase strength, translocation step size and rate, and processivity. *Mf*Lon's ATPase module belongs to the HCLR clade of AAA+ enzymes, which also includes the ClpXP ATPase and the major

Table 1. Quantitative comparisons of mechanical features of three HCLR-clade AAA+ proteases

AAA+ protease	Pre-unfolding dwell (τ, s)			Translocation velocity (mean, nm/s)	Step size (mean, nm) [mode, nm]	ATP per step
	^{V13P}titin^{I27}	^{V15P}titin^{I27}	^{WT}titin^{I27}			
*Mf*Lon[a]	14.0 ± 1.2	ND	ND	2.1 ± 0.2	1.41 ± 0.06 [1]	ND
*Mf*Lon	8.1 ± 0.3	19.6 ± 0.4	51.6 ± 2.7[e]	3.4 ± 0.1	1.66 ± 0.02 [1]	~1
ClpAP[a,b]	1.7 ± 0.2	5.6 ± 0.4	ND	3.0 ± 0.1	1.4 ± 0.5 [1]	ND
ClpXP[a,c]	~5.9	~17.0	~55.0	4.4 ± 0.1	~1–4[d] [1]	~1

Data were taken at 22°C unless indicated otherwise. Errors correspond to ± 1 SEM. ND, not determined.
[a]Dataset taken on dual trap at 18°C.
[b]From Olivares et al.[19]
[c]From Cordova et al.[25]
[d]For ClpXP, most measured steps consisted of multiple 1-nm steps due to kinetic bursts of ATP hydrolysis across multiple subunits.
[e]For the ^{WT}titin^{I27} unfolding dwell time constant for *Mf*Lon, we report a lower threshold value from the time constant of the initial dwell (Figure S3).

AAA+ motor of ClpAP, allowing comparison of the mechanical properties of enzymes differing in structure and subunit composition. Elucidating *Mf*Lon motor properties also highlights unexpected features that likely contribute to Lon's evolutionary versatility.

Lon, ClpAP, and ClpXP use a conserved ~6 residue translocation step

Although *Mf*Lon is a slightly slower unfoldase and translocase than *E. coli* ClpXP or ClpAP, all of these enzymes appear to translocate polypeptides using a ~1-nm core step, corresponding to ~4–8 amino acids (Figures S5A and S5B). Indeed, the probability distribution of step sizes for *Mf*Lon and ClpAP are essentially superimposable (Figure 4B; Table 1).[19] In additional support of this general step size, a single-turnover stop-flow assay estimates the ClpAP step size as ~5 amino acids,[34] and cryo-EM shows movement of exactly 6 substrate residues between two different ClpXP structures bound to the same substrate.[10]

At present, significant controversy exists over the fundamental translocation step of AAA+ unfoldases. Because the pore-1 loops of all known AAA+ protein-translocation motors with high-resolution structures interact with two-residue segments of polypeptide in their axial channels, a two-residue translocation step has been proposed (for review, see Puchades et al.[35]). Although this "structure-inspired" model is still popular, we know of no supporting experimental evidence. By contrast, for both *Mf*Lon and *E. coli* ClpXP, the average time per ~6-residue step (the step dwell) is similar to the average time required by these enzymes to hydrolyze one ATP, with values of ~0.4–0.5 s for *Mf*Lon (this work, at 22°C) and ~0.6 s for ClpXP (at 18°C).[25] This correspondence of times is important, as two-residue steps, if they occur, are below the position resolution limits of our optical-trapping acquisition settings. Thus, the temporal correspondence weighs heavily in support of the ~6-residue translocation step model. Consequently, even if "true" two-residue steps are not detected, then *Mf*Lon (as well as ClpXP) does not hydrolyze ATP fast enough to translocate at the rate expected for a two-residue power stroke. For example, the titin^{I27} domain is ~90 residues, and thus *Mf*Lon would require ~45 two-residue steps for complete translocation. It would therefore take ~18 s to hydrolyze 45 ATPs and translocate the complete titin^{I27} domain in two-residue increments. We observe, however, translocation of entire titin^{I27} domains in 4–5 s in our single-molecule experiments, a rate inconsistent with the two-residue step model. Furthermore, the clearly visible, relatively common apparent "step transitions" of 2–3 nm each correspond to 8–24 amino acids, which would require hydrolysis of 4–12 ATP molecules by the two-residue step model. As these transitions occur within 20 ms, an ATPase rate of at least 200 ATP hydrolyzed per second would be required, which is much faster than observed with *Mf*Lon under any conditions.

Because the AAA+ modules of Lon, ClpX, and the major motor domain of ClpA belong to the same evolutionary HCLR clade, it is not surprising that they share a similar translocation mechanism. There are, however, notable structural differences among these enzymes. For example, the AAA+ and peptidase domains of Lon are coresident on the same polypeptide chain, whereas these domains are located on separate subunits for ClpXP, ClpAP, HslUV, and the 26S proteasome. Moreover, Lon, ClpX, HslU, and the 26S proteasome have one AAA+ hexameric unfoldase ring, whereas ClpA is a "double ring" AAA+ unfoldase with one "classic" and one HCLR ATPase module (Figure 6A). Thus, our results indicate that the same basic motor can be embedded in very different structural frameworks.

*Mf*Lon is an unexpectedly strong and processive unfoldase

E. coli Lon ranked as a "weak" unfoldase in experiments challenging AAA+ proteases with substrates of increasing thermodynamic stabilities, positioned well behind ClpXP, ClpAP, and the 26S proteasome.[33] However, *Mf*Lon unfolds and degrades degron-tagged GFP and titin^{I27}, which are difficult proteins to unfold. Moreover, *Mf*Lon is highly processive, and many of our single-molecule traces included a Halo unfolding event, indicating that the entire substrate was degraded (Figures 5A and 5C), even though *Mf*Lon is a slower translocase and unfoldase than other AAA+ proteases. Ensemble degradation assays also revealed that *Mf*Lon, once it initiates degradation, often degrades the entire substrate, although this "success rate" decreases for the ^{WT}titin$^{I27}{}_4$ substrate, especially at lower reaction temperatures (Figures 5B and S7).

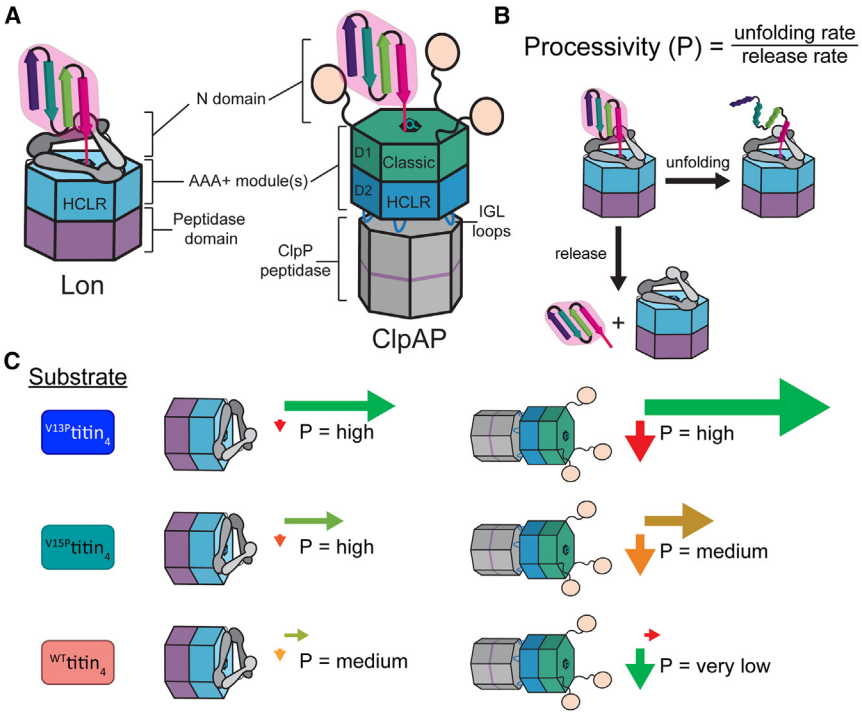

Figure 6. Model for the distinct processivities of *Mf*Lon and *E. coli* ClpAP

(A) Comparison of domain and subunit arrangement for Lon and ClpAP. Each enzyme has six N domains, but only three are shown for clarity. The IGL loops (blue) of ClpA bind in clefts on a heptameric ring of ClpP.

(B) Model explaining degradation of titin^{I27} substrates by *Mf*Lon and *E. coli* ClpAP. P is a processivity factor (rounds of catalysis per substrate association), with higher values corresponding to more complete degradation.

(C) Degradation by Lon or ClpAP of the three multidomain substrates. The length and thickness of the colored arrows for the unfolding rate (rightward arrow) and release rate (downward arrow) represent the approximate relative magnitudes. Green arrows highlight whether unfolding or release is likely to predominate, yellow and orange arrows indicate intermediate probabilities, and red arrows mark unlikely reactions.

The rate and success of protein degradation by AAA+ proteases depends on specific properties of both enzymes and substrates. Important substrate features include (1) areas of high local mechanical stability, especially in the region first encountered by the unfoldase; (2) the protein's fold; (3) the placement of sequences that can be gripped well by the enzymes; and (4) the degron location and the direction of protein degradation.[36] We know less about the critical enzyme characteristics; however, the rate of an enzyme's power stroke/ATPase cycle and its ability to take rapid bursts of multiple steps are two enzyme features that influence its success in degrading some proteins.[19,25,21,37,38] Our current characterization of *Mf*Lon highlights a third important enzyme property, namely the time the protease remains associated with the substrate. In this regard, *Mf*Lon is remarkable compared with other AAA+ proteases analyzed by optical trapping in remaining associated with and continuing to process substrates for unusually long times.[12,19,20,25]

The model of Figure 6 summarizes results of degradation of different titin^{I27} substrates by *Mf*Lon and *E. coli* ClpAP, depicting outcomes based on two unimolecular rates: (1) unfolding for each enzyme/substrate pair and (2) enzyme-substrate disassociation. The ratio of these rates gives a processivity number (P), where high values correspond to frequent degradation of the entire substrate. In contrast to the measured time constants for unfolding, we have no direct measurements of dissociation. However, based on the observed long trace lifetimes, as well as the lower frequency of aborted truncated degradation products appearing in bulk assays, we propose that *Mf*Lon dissociates more slowly than ClpAP. Although enzyme dissociation may depend on features of both the enzyme and the substrate, Figure 6 illustrates the simple case where this rate is an intrinsic property of each enzyme. Inspection of the predicted degradation outcomes illustrates how judging which enzyme is "better/stronger" depends on these rates and the substrate tested. For degradation of either single- or multi-domain ^{V13P}titin^{I27}, ClpAP would clearly appear more successful, as unfolding is faster, and the dissociation rate of either enzyme does not contribute to the outcome. However, with ^{V15P}titin^{I27}, the situation is more complex: on a single-domain substrate, ClpAP would appear "stronger" because it unfolds faster than *Mf*Lon, whereas on a multi-domain variant, *Mf*Lon would be more successful at completing degradation due to slower dissociation. Furthermore, for degradation of ^{WT}titin^{I27}, *Mf*Lon is the superior protease by this scheme, as ClpAP's faster dissociation does not allow it frequent chances to unfold this protein.

Reasonably strong unfolding and high processivity are likely to be important for Lon's degradation of proteins in the Mycoplasma niche, where other cytoplasmic AAA+ proteases are not available to degrade stable substrates that might be toxic or need to be recycled. Regardless, the activities of *Mf*Lon establish that Lon-family enzymes need not be weak unfoldases. Previous studies show that *E. coli* Lon has similar maximum degradation rates to *Mf*Lon,[22] suggesting that divergence in substrate recognition/repertoire between these enzymes likely does not affect the core mechanism of the Lon motor. Moreover, *E. coli* Lon and *Mf*Lon have similar concentration-dependent trends of ATPase and degradation activity, which is a pattern previously observed for *E. coli* Lon and was attributed to a change in oligomeric state (Figures S1A and S1B),[39] further supporting that our findings with *Mf*Lon are likely generalizable to other Lon homologs.

Limitations of the study

Although our model of Lon's processivity satisfies the ensemble and single-molecule results using the *Mf*Lon system, we acknowledge that evolutionary tuning of the enzyme's substrate

specificity may also reflect differences in the degradation parameters for Lon proteases in other bacteria, making these results less generalizable. Moreover, despite analyzing the single-molecule stepping data using two threshold values, there is a technical limitation to the step size that can be detected by this method. If two-residue steps are occurring, they would not be visualized by optical trapping.

STAR★METHODS

Detailed methods are provided in the online version of this paper and include the following:

- KEY RESOURCES TABLE
- RESOURCE AVAILABILITY
  - Lead contact
  - Materials availability
  - Data and code availability
- EXPERIMENTAL MODEL AND STUDY PARTICIPANT DETAILS
  - Bacterial strains
- METHOD DETAILS
  - Protein expression and purification
  - Biochemical assays
  - Single-molecule optical trapping
- QUANTIFICATION AND STATISTICAL ANALYSIS
  - Single-molecule data analysis

SUPPLEMENTAL INFORMATION

Supplemental information can be found online at https://doi.org/10.1016/j.celrep.2023.113061.

ACKNOWLEDGMENTS

We thank Harris Manning and Juan Carlos Cordova for early development of the single-bead assay and Adrian Olivares, Steven Walker, and Mark Hilton for advice and helpful discussions. Barbara Imperiali generously provided the sortase materials. This work was supported by NIH grants AI-016892 (R.T.S. and T.A.B.), DK-115558 (T.A.B.), and T32-GM-007287 (MIT Biology) and the MIT School of Science Service Fellowship (M.R.K.).

AUTHOR CONTRIBUTIONS

Conceptualization, methodology, validation, and funding acquisition, M.R.K., R.T.S., and T.A.B.; investigation, formal analysis, and visualization, M.R.K.; resources, M.R.K., H.C.K., M.M.J., and H.M.S.; writing – original draft, M.R.K. and T.A.B.; writing – review and editing, M.R.K., H.C.K., M.M.J., H.M.S., M.J.L., R.T.S., and T.A.B.; supervision and project administration, T.A.B., R.T.S., and M.J.L.

DECLARATION OF INTERESTS

The authors declare no competing interests.

INCLUSION AND DIVERSITY

We support inclusive, diverse, and equitable conduct of research.

Received: March 2, 2023
Revised: July 15, 2023
Accepted: August 16, 2023

REFERENCES

1. Hoskins, J.R., Kim, S.Y., and Wickner, S. (2000). Substrate Recognition by the ClpA Chaperone Component of ClpAP Protease. J. Biol. Chem. *275*, 35361–35367. https://doi.org/10.1074/jbc.M006288200.
2. Baker, T.A., and Sauer, R.T. (2006). ATP-dependent proteases of bacteria: recognition logic and operating principles. Trends Biochem. Sci. *31*, 647–653. https://doi.org/10.1016/j.tibs.2006.10.006.
3. Gur, E., and Sauer, R.T. (2008a). Recognition of misfolded proteins by Lon, a AAA(+) protease. Genes Dev. *22*, 2267–2277. https://doi.org/10.1101/gad.1670908.
4. Sauer, R.T., and Baker, T.A. (2011). AAA+ proteases: ATP-fueled machines of protein destruction. Annu. Rev. Biochem. *80*, 587–612. https://doi.org/10.1146/annurev-biochem-060408-172623.
5. Tzeng, S.R., Tseng, Y.C., Lin, C.C., Hsu, C.Y., Huang, S.J., Kuo, Y.T., and Chang, C.I. (2021). Molecular insights into substrate recognition and discrimination by the N-terminal domain of Lon AAA+ protease. Elife *10*, e64056. https://doi.org/10.7554/eLife.64056.
6. Yamada-Inagawa, T., Okuno, T., Karata, K., Yamanaka, K., and Ogura, T. (2003). Conserved Pore Residues in the AAA Protease FtsH Are Important for Proteolysis and Its Coupling to ATP Hydrolysis. J. Biol. Chem. *278*, 50182–50187. https://doi.org/10.1074/jbc.M308327200.
7. Siddiqui, S.M., Sauer, R.T., and Baker, T.A. (2004). Role of the processing pore of the ClpX AAA+ ATPase in the recognition and engagement of specific protein substrates. Genes Dev. *18*, 369–374. https://doi.org/10.1101/gad.1170304.
8. Graef, M., and Langer, T. (2006). Substrate specific consequences of central pore mutations in the i-AAA protease Yme1 on substrate engagement. J. Struct. Biol. *156*, 101–108. https://doi.org/10.1016/j.jsb.2006.01.009.
9. Martin, A., Baker, T.A., and Sauer, R.T. (2008b). Pore loops of the AAA+ ClpX machine grip substrates to drive translocation and unfolding. Nat. Struct. Mol. Biol. *15*, 1147–1151. https://doi.org/10.1038/nsmb.1503.
10. Fei, X., Bell, T.A., Barkow, S.R., Baker, T.A., and Sauer, R.T. (2020). Structural basis of ClpXP recognition and unfolding of ssrA-tagged substrates. Elife *9*, e61496. https://doi.org/10.7554/eLife.61496.
11. Kenniston, J.A., Baker, T.A., Fernandez, J.M., and Sauer, R.T. (2003). Linkage between ATP consumption and mechanical unfolding during the protein processing reactions of an AAA+ degradation machine. Cell *114*, 511–520. https://doi.org/10.1016/S0092-8674(03)00612-3.
12. Aubin-Tam, M.-E., Olivares, A.O., Sauer, R.T., Baker, T.A., and Lang, M.J. (2011). Single-molecule protein unfolding and translocation by an ATP-fueled proteolytic machine. Cell *145*, 257–267. https://doi.org/10.1016/j.cell.2011.03.036.
13. Olivares, A.O., Baker, T.A., and Sauer, R.T. (2016). Mechanistic insights into bacterial AAA+ proteases and protein-remodeling machines. Nat. Rev. Microbiol. *14*, 33–44. https://doi.org/10.1038/nrmicro.2015.4.
14. Kowit, J.D., and Goldberg, A.L. (1977). Intermediate steps in the degradation of a specific abnormal protein in Escherichia coli. J. Biol. Chem. *252*, 8350–8357.
15. Ishii, Y., and Amano, F. (2001). Regulation of SulA cleavage by Lon protease by the C-terminal amino acid of SulA, histidine. Biochem. J. *358*, 473–480. https://doi.org/10.1042/bj3580473.
16. Tsilibaris, V., Maenhaut-Michel, G., and Van Melderen, L. (2006). Biological roles of the Lon ATP-dependent protease. Res. Microbiol. *157*, 701–713. https://doi.org/10.1016/j.resmic.2006.05.004.
17. Gur, E., and Sauer, R.T. (2008b). Evolution of the ssrA degradation tag in Mycoplasma: Specificity switch to a different protease. Proc. Natl. Acad. Sci. USA *105*, 16113–16118. https://doi.org/10.1073/pnas.0808802105.
18. Ge, Z., and Karzai, A.W. (2009). Co-evolution of multipartite interactions between an extended tmRNA tag and a robust Lon protease in Mycoplasma. Mol. Microbiol. *74*, 1083–1099. https://doi.org/10.1111/j.1365-2958.2009.06923.x.

19. Olivares, A.O., Nager, A.R., Iosefson, O., Sauer, R.T., and Baker, T.A. (2014). Mechanochemical basis of protein degradation by a double-ring AAA+ machine. Nat. Struct. Mol. Biol. *21*, 871–875. https://doi.org/10.1038/nsmb.2885.

20. Kotamarthi, H.C., Sauer, R.T., and Baker, T.A. (2020). The Non-dominant AAA+ Ring in the ClpAP Protease Functions as an Anti-stalling Motor to Accelerate Protein Unfolding and Translocation. Cell Rep. *30*, 2644–2654.e3. https://doi.org/10.1016/j.celrep.2020.01.110.

21. Nager, A.R., Baker, T.A., and Sauer, R.T. (2011). Stepwise unfolding of a β barrel protein by the AAA+ ClpXP protease. J. Mol. Biol. *413*, 4–16. https://doi.org/10.1016/j.jmb.2011.07.041.

22. Wohlever, M.L., Nager, A.R., Baker, T.A., and Sauer, R.T. (2013). Engineering fluorescent protein substrates for the AAA+ Lon protease. Protein Eng. Des. Sel. *26*, 299–305. https://doi.org/10.1093/protein/gzs105.

23. Carrion-Vazquez, M., Oberhauser, A.F., Fowler, S.B., Marszalek, P.E., Broedel, S.E., Clarke, J., and Fernandez, J.M. (1999). Mechanical and chemical unfolding of a single protein: A comparison. Proc. Natl. Acad. Sci. USA *96*, 3694–3699. https://doi.org/10.1073/pnas.96.7.3694.

24. Li, H., Carrion-Vazquez, M., Oberhauser, A.F., Marszalek, P.E., and Fernandez, J.M. (2000). Point mutations alter the mechanical stability of immunoglobulin modules. Nat. Struct. Biol. *7*, 1117–1120. https://doi.org/10.1038/81964.

25. Cordova, J.C., Olivares, A.O., Shin, Y., Stinson, B.M., Calmat, S., Schmitz, K.R., Aubin-Tam, M.-E., Baker, T.A., Lang, M.J., and Sauer, R.T. (2014). Stochastic but highly coordinated protein unfolding and translocation by the ClpXP proteolytic machine. Cell *158*, 647–658. https://doi.org/10.1016/j.cell.2014.05.043.

26. Cormack, B.P., Valdivia, R.H., and Falkow, S. (1996). FACS-optimized mutants of the green fluorescent protein (GFP). Gene *173*, 33–38. https://doi.org/10.1016/0378-1119(95)00685-0.

27. Kim, Y.I., Burton, R.E., Burton, B.M., Sauer, R.T., and Baker, T.A. (2000). Dynamics of substrate denaturation and translocation by the ClpXP degradation machine. Mol. Cell *5*, 639–648. https://doi.org/10.1016/S1097-2765(00)80243-9.

28. Maillard, R.A., Chistol, G., Sen, M., Righini, M., Tan, J., Kaiser, C.M., Hodges, C., Martin, A., and Bustamante, C. (2011). ClpX(P) Generates Mechanical Force to Unfold and Translocate Its Protein Substrates. Cell *145*, 459–469. https://doi.org/10.1016/j.cell.2011.04.010.

29. Olivares, A.O., Kotamarthi, H.C., Stein, B.J., Sauer, R.T., and Baker, T.A. (2017). Effect of directional pulling on mechanical protein degradation by ATP-dependent proteolytic machines. Proc. Natl. Acad. Sci. USA *114*, E6306–E6313. https://doi.org/10.1073/pnas.1707794114.

30. Greenleaf, W.J., Woodside, M.T., Abbondanzieri, E.A., and Block, S.M. (2005). Passive All-Optical Force Clamp for High-Resolution Laser Trapping. Phys. Rev. Lett. *95*, 208102. https://doi.org/10.1103/PhysRevLett.95.208102.

31. Kerssemakers, J.W.J., Munteanu, E.L., Laan, L., Noetzel, T.L., Janson, M.E., and Dogterom, M. (2006). Assembly dynamics of microtubules at molecular resolution. Nature *442*, 709–712. https://doi.org/10.1038/nature04928.

32. Gur, E., and Sauer, R.T. (2009). Degrons in protein substrates program the speed and operating efficiency of the AAA+ Lon proteolytic machine. Proc. Natl. Acad. Sci. USA *106*, 18503–18508. https://doi.org/10.1073/pnas.0910392106.

33. Koodathingal, P., Jaffe, N.E., Kraut, D.A., Prakash, S., Fishbain, S., Herman, C., and Matouschek, A. (2009). ATP-dependent proteases differ substantially in their ability to unfold globular proteins. J. Biol. Chem. *284*, 18674–18684. https://doi.org/10.1074/jbc.M900783200.

34. Miller, J.M., Lin, J., Li, T., and Lucius, A.L. (2013). E. coli ClpA catalyzed polypeptide translocation is allosterically controlled by the protease ClpP. J. Mol. Biol. *425*, 2795–2812. https://doi.org/10.1016/j.jmb.2013.04.019.

35. Puchades, C., Sandate, C.R., and Lander, G.C. (2020). The molecular principles governing the activity and functional diversity of AAA+ proteins. Nat. Rev. Mol. Cell Biol. *21*, 43–58. https://doi.org/10.1038/s41580-019-0183-6.

36. Lee, C., Schwartz, M.P., Prakash, S., Iwakura, M., and Matouschek, A. (2001). ATP-dependent proteases degrade their substrates by processively unraveling them from the degradation signal. Mol. Cell *7*, 627–637. https://doi.org/10.1016/S1097-2765(01)00209-X.

37. Martin, A., Baker, T.A., and Sauer, R.T. (2005). Rebuilt AAA + motors reveal operating principles for ATP-fuelled machines. Nature *437*, 1115–1120. https://doi.org/10.1038/nature04031.

38. Martin, A., Baker, T.A., and Sauer, R.T. (2008a). Protein unfolding by a AAA+ protease is dependent on ATP-hydrolysis rates and substrate energy landscapes. Nat. Struct. Mol. Biol. *15*, 139–145. https://doi.org/10.1038/nsmb.1380.

39. Vieux, E.F., Wohlever, M.L., Chen, J.Z., Sauer, R.T., and Baker, T.A. (2013). Distinct quaternary structures of the AAA+ Lon protease control substrate degradation. Proc. Natl. Acad. Sci. USA *110*, E2002–E2008. https://doi.org/10.1073/pnas.1307066110.

STAR★METHODS

KEY RESOURCES TABLE

REAGENT or RESOURCE	SOURCE	IDENTIFIER
Antibodies		
Anti-Digoxigenin, polyclonal antibody, immunoglobulin	Sigma Aldrich	Cat# 11333089001; RRID: AB_514496
Bacterial and virus strains		
BL21(DE3)	New England Biolabs	C2527H
ElectroMAX^{TM} DH5α-E Competent Cells	Invitrogen	11319019
Chemicals, peptides, and recombinant proteins		
*Mf*ssrA peptide for sortase ligation	21st Century Biochemicals	N/A
Glass Binding Peptide CGGRSGRRRSHHHRL	Synthesized using Fmoc technique and in Apex 396 solid-phase peptide synthesizer	N/A
HaloTag Succinimidyl Ester Ligand O4	Promega	P6751
Sulfosuccinimidyl 4-[N-maleimidomethyl] cyclohexane-1-carboxylate	Thermo Scientific	PI22622
Glucose Oxidase, Aspergillus niger, Recombinant	EMD Millipore	345386
Catalase from bovine liver	Sigma Aldrich	C30
Bovine serum albumin	New England Biolabs	B9000S
mPEG-Silane, MW 5000	Laysan Bio	MPEG-SIL-5000
Biotin-PEG-Silane, MW 5000	Laysan Bio	Biotin-PEG-SIL-5K
EDC (1-ethyl-3-(3-dimethylaminopropyl) carbodiimide hydrochloride) crosslinker	Thermo Scientific	22980
Streptavidin	EMD Millipore	189730
Oligonucleotides		
M13MP18 double stranded DNA	Bayou Biolabs	P-105
5BiosG/AATCCGCTTTGCTTCTGAC	IDTDNA, USA	N/A
5AmMC6/TTGAAATACCGACCGTGTG	IDTDNA, USA	N/A
5DigN/TATTGCGTTTCCTCGGTTTC	IDTDNA, USA	N/A
5AmMC12/TTGAAATACCGACCGTGTGA	IDTDNA, USA	N/A
Recombinant DNA		
pBAD33 plasmid containing *Mf*Lon	Gur and Sauer, 2008b[9]	N/A
pFN18A plasmid containing Halo-V13P$_3$-LPETGG-His$_6$	This study, derived from Cordova et al., 2014[25]	N/A
pFN18A plasmid containing Halo-V13P$_4$-LPETGG-His$_6$	This study, derived from Cordova et al., 2014[25]	N/A
pFN18A plasmid containing Halo-V15P$_4$-LPETGG-His$_6$	This study, derived from Cordova et al., 2014[25]	N/A
pFN18A plasmid containing Halo-WT$_4$-LPETGG-His$_6$	This study, derived from Cordova et al., 2014[25]	N/A
pFN18A plasmid containing Halo-WT$_{4.125}$-LPETGG-His$_6$	This study, derived from Cordova et al., 2014[25]	N/A
pET28b plasmid containing GFPmut3-LPETGG-His$_6$	This study	N/A
pET28b plasmid containing cp7-^{SF}GFP-LPETGG-His$_6$	This study, derived from Nager et al., 2011[21]	N/A
pET23b plasmid containing SUMO-V13P-LPETGG-His$_6$	This study	N/A
pET23b plasmid containing SUMO-V15P-LPETGG-His$_6$	This study	N/A
pET23b plasmid containing SUMO-WT-LPETGG-His$_6$	This study	N/A
pET23b plasmid containing SUMO-WT$_{1.125}$-LPETGG-His$_6$	This study	N/A

(*Continued on next page*)

Continued		
REAGENT or RESOURCE	SOURCE	IDENTIFIER
Software and algorithms		
Step finding algorithm	Kerssemakers et al., 2006[31]	https://doi.org/10.1038/nature04928
XLSTAT	Addinsoft 2022	https://www.xlstat.com/en/solutions/basic
Other		
1.25 μm streptavidin coated polystyrene beads	Spherotech	SVP-10-5 1%w/v, 1.25
1.09 μm streptavidin coated polystyrene beads	Spherotech	SVP-10-5 1%w/v, 1.09
1.09 μm carboxylate polystyrene beads	Polysciences, Inc.	08226

RESOURCE AVAILABILITY

Lead contact

Further information and requests for resources and reagents should be directed to and will be fulfilled by the lead contact, Tania Baker (tabaker@mit.edu).

Materials availability

This study generated unique plasmids for the *Mf*Lon(T786C) enzyme and sortase-ligated substrates. Further information and requests for resources will be fulfilled by the lead contact upon MTA completion.

Data and code availability

- All datasets generated and analyzed in this study and reported in this paper are available from the lead contact by reasonable request.
- This paper does not report original code.
- Any additional information required to reanalyze the data reported in this paper is available from the lead contact upon request.

EXPERIMENTAL MODEL AND STUDY PARTICIPANT DETAILS

Bacterial strains

*Mf*Lon(T786C), *Mf*Lon, Halo-^{V13P}titin$^{I27}{}_3$-LPETGG-His$_6$, Halo-^{V13P}titin$^{I27}{}_4$-LPETGG-His$_6$, Halo-^{V15P}titin$^{I27}{}_4$-LPETGG-His$_6$, Halo-^{WT}titin$^{I27}{}_4$-LPETGG-His$_6$, and Halo-^{WT}titin$^{I27}{}_4$-linker-LPETGG-His$_6$ were expressed in *E. coli* BL21(DE3) strain. Cells were grown between 33°C and 37°C. Exact growth conditions, expression protocols, and purification methods are given in method details.

METHOD DETAILS

Protein expression and purification

*Mf*Lon and *Mf*Lon(T786C) were cloned into pBAD33 vectors and transformed into *E. coli* BL21(DE3) expression cells. Cells were grown to OD_{600} = 1.0 in LB broth at 37°C and expression was initiated with 0.2% w/v L-arabinose. The cells were harvested 3 h later by centrifugation at 4000x*g* and then flash frozen in liquid-N_2 and stored at −80°C. The pellet was resuspended in MF Buffer (25 mM HEPES-KOH, pH 7.5, 100 mM KCl, 10 mM $MgCl_2$, 1 mM DTT) and lysed using a French press at 26 kPSI and centrifuged for 45 min at 30,000x*g* before decanting the supernatant into a Falcon tube containing 10 mg/mL streptomycin sulfate. This mixture was incubated for 1 h at 4°C while rocking to precipitate nucleic acids and then centrifuged again for 45 min at 30,000x*g*. The supernatant was loaded onto a 25 mL hydroxylapatite (HAP) column equilibrated in MF Buffer. The HAP column was washed with two column volumes (CV) of MF Buffer and developed with a linear potassium phosphate (pH 7.5) gradient from 0 to 0.5 M over 10 CV. Fractions containing *Mf*Lon were pooled, and buffer exchanged into Mono Q Buffer A (50 mM HEPES-KOH, pH 7.5, 100 mM KCl, 10 mM $MgCl_2$, 1 mM DTT) using a HiPrep 26/10 column. The sample was passed through a 0.22 μm filter and loaded onto a pre-equilibrated Mono Q 10/100 column. *Mf*Lon was eluted using a 0 to 0.5 M KCl gradient over 20 CV. Fractions containing *Mf*Lon were pooled and loaded onto a Superdex 200 16/600 gel filtration column pre-equilibrated with MF Buffer. Fractions containing *Mf*Lon were pooled, concentrated using an Amicon concentrator (30 kDa cutoff), aliquoted, flash frozen with liquid-N_2, and stored at −80°C.

Titin^{I27} substrates were cloned into pFN18A vectors and transformed into *E. coli* BL21(DE3). Cells were grown at 37°C to OD_{600} = 0.6 in LB broth, chilled to 25°C, and induced with 1 mM isopropyl β-D-1-thiogalactopyranoside (IPTG). The cells were harvested 3 h later by centrifugation (4000x*g*) and then flash frozen in liquid-N_2 and stored at −80°C. The pellet was resuspended in I27 Lysis Buffer (50 mM sodium phosphate buffer, pH 8, 500 mM NaCl, 10% glycerol, 20 mM imidazole) and lysed using a French press at 26 kPSI. The lysate was supplemented with 2 mM $MgCl_2$, 2 μL benzonase per 30 mL cells, and 10 μL protease cocktail inhibitor and then

centrifuged for 45 min at 30,000x*g*. The supernatant was decanted and incubated for 1 h while rocking at 4°C with pre-equilibrated Ni-NTA resin (2 mL CV per L cells) in I27 Lysis Buffer. The flow through was collected by gravity flow and the resin was washed with 60 CV of I27 Lysis Buffer. The substrate was eluted with I27 Elution Buffer (50 mM sodium phosphate buffer, pH 8, 500 mM NaCl, 10 mM $MgCl_2$, 10% glycerol, 250 mM imidazole). Fractions containing substrate were passed through a 0.22 μm filter and loaded onto a pre-equilibrated Superdex 75 16/60 column in MF Buffer containing 0.1 mM EDTA. Fractions containing substrate were concentrated using an Amicon concentrator (10 kDa cutoff), aliquoted, flash frozen using liquid-N_2, and stored at −80°C.

GFP substrates were cloned into pET28b vectors and transformed into *E. coli* BL21(DE3). Cells were grown at 33°C to OD_{600} = 0.6 in LB broth, chilled to 22°C, and induced with 0.5 mM IPTG. After overnight induction, the cells were harvested (4000x*g*), flash frozen in liquid-N_2, and stored at −80°C. The pellet was resuspended in GFP Lysis Buffer (25 mM Tris-HCl, pH 7.5, 180 mM KCl, 20 mM imidazole, 10% glycerol, 1 mM DTT) and lysed using a French press at 26 kPSI. The lysate was supplemented with 2 μL benzonase per 30 mL cells and 10 μL protease cocktail inhibitor and then centrifuged for 45 min at 30,000x*g*. The supernatant was decanted and incubated for 1 h while rocking at 4°C with pre-equilibrated Ni-NTA resin (2 mL CV per L cells) in GFP Lysis Buffer. The flow through was collected by gravity flow and the resin was washed with 20 CV of GFP Lysis Buffer. The substrate was eluted with GFP Elution Buffer (25 mM Tris-HCl, pH 7.5, 200 mM KCl, 300 mM imidazole, 10% glycerol, 1 mM DTT). Fractions containing substrate were passed through a 0.22 μm filter and loaded onto a pre-equilibrated Superdex 75 16/60 column in MF Buffer containing 0.1 mM EDTA. Fractions containing substrate were concentrated using an Amicon concentrator (10 kDa cutoff), aliquoted, flash frozen with liquid-N_2, and stored at −80°C.

Biochemical assays

Titin^{I27}-*Mf*ssrA degradation was assayed at 22°C–30°C by tracking the disappearance of substrate over time by SDS-PAGE gel. Final concentrations were 150 nM *Mf*Lon_6, 3–15 μM substrate, 3–15 μM HaloTag TMR ligand, 5 mM ATP, 12.5 mM phosphoenolpyruvate (PEP), and 23.4 units/mL pyruvate kinase (PK) in MF Buffer. The TMR ligand was visualized using a Typhoon imager (excitation 532 nm) and band density was determined using ImageQuant software. GFP-*Mf*ssrA and cp7-^{SF}GFP-*Mf*ssrA degradation was assayed at 30°C by following loss of fluorescence (excitation, 467 nm; emission, 511 nm). Final concentrations were 150 nM *Mf*Lon_6, 0.5–30 μM substrate, 2% DMSO, 5 mM ATP, 5 mM phosphocreatine (CP), and 0.05 mg/mL creatine kinase (CK) in MF Buffer. Steady-state ATP hydrolysis at 22°C–30°C was monitored by loss of NADH absorbance at 340 nm with final concentrations of 150 nM *Mf*Lon_6, 0–35 μM substrate, 5 mM ATP, 18.75 U/mL PK, 21.45 U/mL lactose dehydrogenase (LDH), 5 mM PEP, and 0.875 mM NADH in MF Buffer.

For carboxymethylation, ^{V13P}titin^{I27} and ^{V15P}titin^{I27} were unfolded in 6 M guanidinium hydrochloride for 2 h and then reacted with 4 mM iodoacetamide for 2 h. The modified proteins were then exchanged into MF Buffer and concentrated using a 10-kDa cutoff Amicon concentrator.

Single-molecule optical trapping

Purified *Mf*Lon(T786C) at 1–10 mg/mL was buffer exchanged into degassed Maleimide Reaction Buffer (20 mM potassium phosphate, pH 7.2, 100 mM KCl, 10 mM $MgCl_2$) using a PD-10 Desalting column and incubated in a tube covered with aluminum foil for 2 h at room temperature with a 20-fold molar excess of EZ-link maleimide-PEG2-biotin resuspended in 100% DMSO. Excess reagent was removed, and the enzyme was exchanged into MF Buffer using a PD-10 Desalting column. Halo multi-domain substrates were incubated with HaloTag succinylester ligand-1010bp DNA-digoxigenin at 4°C overnight while rotating in a covered tube.

A 12-μL flow cell was made using two pieces of double-sided tape spaced ~0.5 cm apart on a glass slide and covered with a biotin-pegylated KOH-etched coverslip. The chamber was incubated with 0.1 mg/mL streptavidin in PBS buffer (10 mM sodium phosphate, pH 7.4, 1.8 mM potassium phosphate, pH 7.4, 137 mM NaCl, 2.7 mM KCl) and washed with 100 μL PD buffer (50 mM HEPES, pH 7.6, 200 mM KCl, 10 mM $MgCl_2$, 1 mM DTT). Biotinylated *Mf*Lon^{T786C} was tethered to the coverslip by flowing in 12 μL of the enzyme in PBS with 5 mM ATP, 12.5 mM PEP, and 2.34 units PK. Washed and vortexed anti-digoxigenin-coated 1.09 μm polystyrene beads in PD buffer were added to the substrate-DNA mixture and incubated for 30–60 min. Substrate-coated beads were spun down at 8000x*g* for 2 min, resuspended in 1 mg/mL BSA, spun down again, and resuspended in Imaging Buffer (25.2 μL PD buffer, 3.6 μL ATP Regeneration Mix (5 mM ATP, 12.5 mM PEP, and 23.4 units/mL PK), 0.3 μL 25 mg/mL glucose oxidase, 0.3 μL 3 mg/mL catalase, and 0.6 μL 250 mg/mL glucose). The substrate-coated beads were added to the flow chamber which was sealed with Krytox GPL 206 Grease.

A stiff laser trap was used to capture a substrate-coated bead in solution and moved to just above the surface. The piezo stage was moved in the positive or negative x- or y-direction to scan the surface of the slide for a surface-tethered *Mf*Lon enzyme. Stable tethers were formed when a bead-bound substrate was recognized and engaged by a molecule of surface-tethered *Mf*Lon. The movement of the bead within the laser beam was monitored to follow the translocation and unfolding of the substrate by the enzyme. Upon tether formation, the bead was pulled out of the center of the laser beam by *Mf*Lon and the bead position was monitored as the enzyme processively degraded the multi-domain substrate. All single-molecule experiments were conducted at room temperature (21°C–22°C).

Due to the geometry of the assay components, the trapping force on the bead that maintains its position in the center of the laser beam, which is the force recorded by the instrument throughout an experimental trace, is not necessarily the same force that the substrate experiences during mechanical unfolding and translocation. It is this second force that is most relevant for understanding

the biophysics of Lon's mechanical processing of the substrate, and the wormlike chain model (WLC) was therefore used to calculate the force needed to stretch an unfolded titin^{I27} polypeptide chain to the observed extension length.[20] This calculated value reports on the theoretical forces being experienced by the substrate protein while collecting the experimental trace.

QUANTIFICATION AND STATISTICAL ANALYSIS

Single-molecule data analysis

Data acquisition was carried out as described[12,19,25] but modified for the single-bead assay: initial processing was done using MATLAB scripts used to calculate bead-to-surface distances as described previously for the dual-trap assay bead-to-bead distances. PUD times were determined by finding the derivative of the trace and identifying the inflection point as the enzyme finished translocating the previous polypeptide chain and started to attempt to unfold the next folded substrate domain. Translocation rates were determined by calculating the change in bead position divided by the time to complete domain translocation. Data were collected at 3000 or 5000 Hz and decimated to 50 Hz and individual translocation steps were identified using a chi-squared minimization method as described.[25,31] Bootstrap analyses were conducted as described previously.[20] Briefly, to estimate the distribution and error of the PUDs, we carried out nonparametric bootstrap analysis using the XLSTAT statistical analysis tool (Addinsoft 2022; XLSTAT statistical and data analysis, Boston, USA; https://www.xlstat.com/en/). Sample datasets of equal size consisting of randomly-chosen members from the experimental dataset were created (n = 256 iterations) then individually fit to a single or double exponential. R^2 values for the resulting fits were also calculated. Additionally, we reported the 95% confidence intervals of the normally-distributed fitting parameters of all the iterations.